RA-BUSSeg: Relation-aware Semi-supervised Breast Ultrasound Image Segmentation via Adjacent Propagation and Cross-layer Alignment

Supplementary Material

1. Impact of Loss Weights

In the overall loss function, $\mathcal{L} = \mathcal{L}_s + \lambda_u \mathcal{L}_u + \lambda_1 \mathcal{L}_{ARP} + \lambda_2 \mathcal{L}_{CRA}$, the choice of weights λ_1 and λ_2 is crucial. If these weights are excessively high or low, they may hinder the model training process by disrupting the balance of attention across different pixel relations, ultimately exerting a detrimental effect on its performance. Therefore, ensuring a well-coordinated and reasonable setting of λ_1 and λ_2 is essential. Tab. 1 presents the ablation study results for λ_1 and λ_2, indicating that the model achieves its best performance when both parameters are set to 1. This balanced configuration allows each component to contribute effectively to the learning process, thereby enhancing the overall efficacy and robustness of the model.

λ_1	λ_2	UDIAT		BUSI	
		Dice (%)	IoU (%)	Dice (%)	IoU (%)
0.5	0.5	80.32	72.11	76.20	66.96
0.5	1.0	81.40	72.97	76.79	67.52
1.0	0.5	81.73	73.03	77.24	68.39
1.0	1.0	**82.55**	**74.21**	**77.95**	**69.30**
1.5	1.0	82.11	73.47	77.39	68.95
1.0	1.5	81.69	72.42	76.98	67.71
1.5	1.5	80.41	71.58	76.47	67.60

Table 1. Ablation studies in the weights of loss function on the 1/4 partition protocol of UDIAT and BUSI datasets.

2. More Experimental Results

2.1. More results in ablation studies

To intuitively illustrate the effectiveness of each component, we provide additional visual feature maps for comparison, as shown in Fig. 1. The results confirm that incorporating the proposed ARP and CRA modules enhances breast tumor segmentation, producing more complete and accurate results even in challenging scenarios with low contrast, severe artifacts, and substantial variations in size and shape. Furthermore, we present complete quantitative results from ablation studies conducted under the 1/2 and 1/8 partition protocols on two public breast ultrasound datasets, UDIAT[12] (see Tab. 3) and BUSI[1] (see Tab. 2), respectively. These results further validate the effectiveness of the ARP and CRA modules, demonstrating that their progressive integration significantly improves segmentation performance across different partitioning strategies.

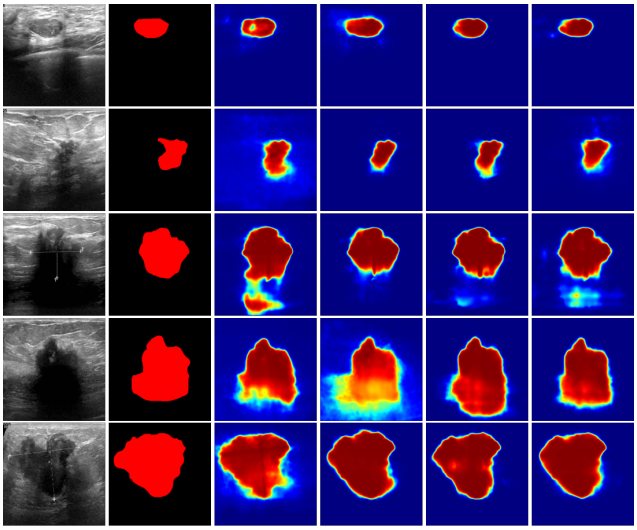

Figure 1. Visual comparison of feature maps in adding ARP and CRA on 1/4 partition protocol of UDIAT and BUSI datasets. (a) Image. (b) GT. (c) SupOnly. (d) w/ ARP. (e) w/ CRA. (f) Ours.

Method		BUSI			
ARP	CRA	1/2		1/8	
		Dice±std (%)	IoU±std (%)	Dice±std (%)	IoU±std (%)
		74.17±2.39	65.60±2.51	68.96±1.86	60.28±1.81
✓		77.51±1.89	68.83±1.40	73.58±1.26	65.18±1.55
	✓	78.08±2.04	69.30±2.30	74.15±1.99	65.72±2.08
✓	✓	**79.11±1.89**	**70.30±2.06**	**75.06±2.19**	**66.41±2.35**

Table 2. Ablation studies of proposed ARP and CRA components on 1/2 and 1/8 partition protocols of BUSI dataset.

Method		UDIAT			
ARP	CRA	1/2		1/8	
		Dice±std (%)	IoU±std (%)	Dice±std (%)	IoU±std (%)
		78.51±1.34	69.55±1.46	72.24±4.13	63.27±4.21
✓		82.80±2.88	74.07±2.93	77.54±4.32	68.45±4.14
	✓	83.13±1.76	74.20±1.81	78.41±4.72	69.48±4.56
✓	✓	**84.77±2.43**	**76.40±2.26**	**79.76±2.79**	**71.24±2.68**

Table 3. Ablation studies of proposed ARP and CRA components on 1/2 and 1/8 partition protocols of UDIAT dataset.

2.2. More visual results in comparison experiments

We provide more visual comparisons against ten state-of-the-art (SOTA) methods on UDIAT and BUSI datasets under 1/2, 1/4 and 1/8 partition protocols. The SOTA methods

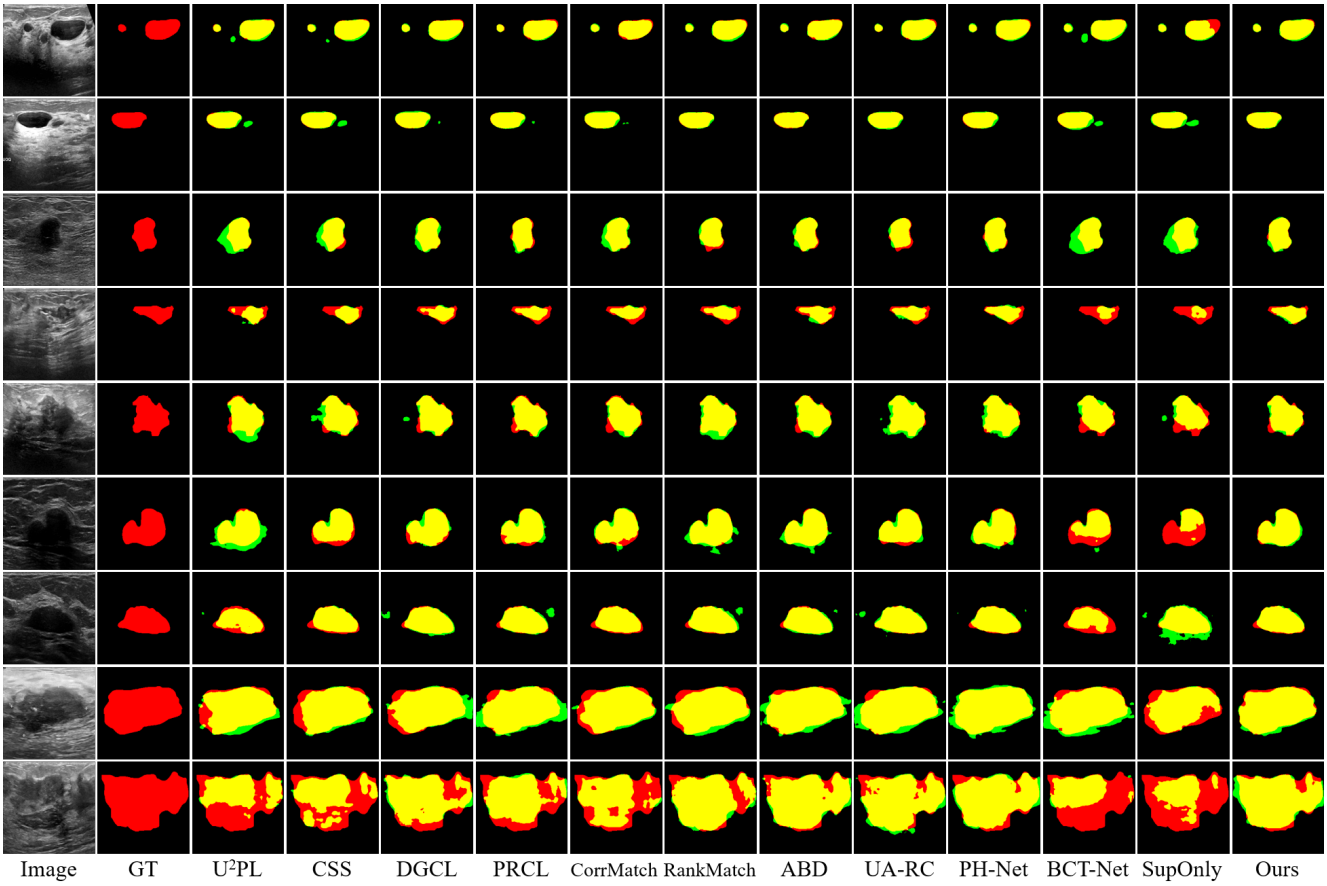

Figure 2. Visual comparison with state-of-the-art methods on the 1/2, 1/4 and 1/8 partition protocols of UDIAT and BUSI datasets. Red, green and yellow regions represent ground truth, prediction and their overlapping regions, respectively.

include (1) seven semi-supervised methods for natural and medical image segmentation: U^{2}PL [8], CSS [6], DGCL [7], PRCL [10], CorrMatch [5], RankMatch [4] and ABD [2]; (2) two semi-supervised breast ultrasound (BUS) image segmentation methods: UA-RC [9] and PH-Net [3]; and (3) a fully-supervised BUS image segmentation method, BCT-Net [11]. As illustrated in the first two samples in Fig. 2, our model accurately detects each lesion in cases containing multiple tumors, ensuring precise identification of tumor counts. Additionally, for the remaining cases in Fig. 2, we intentionally showcase the model's robust segmentation performance across various BUS imaging challenges, including low contrast, speckle noise, and severe artifacts. These examples also encompass lesions of varying sizes, further demonstrating the model's ability to adapt to lesions with diverse scales. These visual results illustrate our model's robustness in handling challenging cases, underscoring its effectiveness and adaptability in practical applications.

3. More Analysis of CRA

As shown in Tab. 4, we provide more ablation studies on the cross-layer relation alignment (CRA) module, with particular focus on proxy sampling strategies and alignment scale configurations.. Three proxy sampling approaches are comparatively analyzed: (1) random sampling is simple, but may limit feature diversity due to its passive nature; (2) clustering is computationally costly, may smooth valuable features, and introduces noise by involving all features; (3) patch-based proxy cannot adapt to lesion scale variations because their quality may highly dependent on patch size. To address these limitations, our approach employs weak cross-correlation to actively identify and leverage highly divergent features, thereby enhancing both proxy diversity and semantic coverage. Furthermore, we investigate the impact of alignment scale numbers. It suggests that increasing the number of aligned layers could facilitate more comprehensive semantic information transfer across different feature levels, potentially yielding further performance enhancements.

Alignment	Proxy	Number of Scales	Sampling Strategy	Dice	HD
✗	✗	-	-	75.11	7.01
✓	✗	4	-	79.09	6.63
✓	✓	4	random	79.83	6.52
✓	✓	4	clustering	80.55	6.39
✓	✓	4	patch-based	80.14	6.34
✓	✓	2	greedy (ours)	79.94	6.54
✓	✓	3	greedy (ours)	80.85	6.05
✓	✓	4	greedy (ours)	**81.21**	**5.99**

Table 4. Detailed ablation studies on CRA module on UDIAT dataset under 1/4 partition. Row 1: baseline. Row 2: global alignment without proxy sampling. Rows 3-5: different proxy sampling strategies. Rows 6-8: different number of scales in alignment.

References

[1] Walid Al-Dhabyani, Mohammed Gomaa, Hussien Khaled, and Aly Fahmy. Dataset of breast ultrasound images. *Data in brief*, 28:104863, 2020. 1

[2] Hanyang Chi, Jian Pang, Bingfeng Zhang, and Weifeng Liu. Adaptive bidirectional displacement for semi-supervised medical image segmentation. In *Proceedings of the IEEE/CVF Conference on Computer Vision and Pattern Recognition*, pages 4070–4080, 2024. 2

[3] Siyao Jiang, Huisi Wu, Junyang Chen, Qin Zhang, and Jing Qin. Ph-net: Semi-supervised breast lesion segmentation via patch-wise hardness. In *Proceedings of the IEEE/CVF Conference on Computer Vision and Pattern Recognition*, pages 11418–11427, 2024. 2

[4] Huayu Mai, Rui Sun, Tianzhu Zhang, and Feng Wu. Rankmatch: Exploring the better consistency regularization for semi-supervised semantic segmentation. In *Proceedings of the IEEE/CVF Conference on Computer Vision and Pattern Recognition*, pages 3391–3401, 2024. 2

[5] Boyuan Sun, Yuqi Yang, Le Zhang, Ming-Ming Cheng, and Qibin Hou. Corrmatch: Label propagation via correlation matching for semi-supervised semantic segmentation. In *Proceedings of the IEEE/CVF Conference on Computer Vision and Pattern Recognition*, pages 3097–3107, 2024. 2

[6] Changqi Wang, Haoyu Xie, Yuhui Yuan, Chong Fu, and Xiangyu Yue. Space engage: Collaborative space supervision for contrastive-based semi-supervised semantic segmentation. In *Proceedings of the IEEE/CVF International Conference on Computer Vision*, pages 931–942, 2023. 2

[7] Xiaoyang Wang, Bingfeng Zhang, Limin Yu, and Jimin Xiao. Hunting sparsity: Density-guided contrastive learning for semi-supervised semantic segmentation. In *Proceedings of the IEEE/CVF Conference on Computer Vision and Pattern Recognition*, pages 3114–3123, 2023. 2

[8] Yuchao Wang, Haochen Wang, Yujun Shen, Jingjing Fei, Wei Li, Guoqiang Jin, Liwei Wu, Rui Zhao, and Xinyi Le. Semi-supervised semantic segmentation using unreliable pseudo-labels. In *Proceedings of the IEEE/CVF conference on computer vision and pattern recognition*, pages 4248–4257, 2022. 2

[9] Yuanchen Wu, Xiaoqiang Li, and Yue Zhou. Uncertainty-aware representation calibration for semi-supervised medical imaging segmentation. *Neurocomputing*, 595:127912, 2024. 2

[10] Haoyu Xie, Changqi Wang, Jian Zhao, Yang Liu, Jun Dan, Chong Fu, and Baigui Sun. Prcl: Probabilistic representation contrastive learning for semi-supervised semantic segmentation. *International Journal of Computer Vision*, pages 1–19, 2024. 2

[11] Junchang Xin, Yaqi Yu, Qi Shen, Shudi Zhang, Na Su, and Zhiqiong Wang. Bct-net: semantic-guided breast cancer segmentation on bus. *Medical & Biological Engineering & Computing*, pages 1–12, 2025. 2

[12] Moi Hoon Yap, Manu Goyal, Fatima Osman, Robert Martí, Erika Denton, Arne Juette, and Reyer Zwiggelaar. Breast ultrasound region of interest detection and lesion localisation. *Artificial Intelligence in Medicine*, 107:101880, 2020. 1